Ultrasound in Med. & Biol., Vol. 29, No. 11, pp. 1561–1570, 2003

0301-5629/03/$–see front matter

ELSEVIER

doi:10.1016/j.ultrasmedbio.2003.08.013

● *Original Contribution*

AN AUTOMATIC APPROACH FOR MORPHOLOGICAL ANALYSIS AND MALIGNANCY EVALUATION OF OVARIAN MASSES USING B-SCANS

YAIR ZIMMER,* RON TEPPER† and SOLANGE AKSELROD*
*Medical Physics Department, Tel Aviv University, Tel Aviv, Israel; and †Ultrasound Unit, Department of Obstetrics and Gynecology, Sapir Medical Center, Kfar Saba, Israel

(*Received* 2 *December* 2002; *revised* 21 *July* 2003; *in final form* 5 *August* 2003)

Abstract—Ovarian masses are a common phenomenon among women of all ages. The importance of prompt diagnosis of ovarian malignancies is obvious, due to the high mortality rate and the difficulty to detect a tumor in its early stages. In this work, an automatic technique for quantitative analysis and malignancy detection of ovarian masses using B-scan ultrasound (US) images is presented. The core of the technique is morphologic analysis of the ovarian mass. The method employed for this task is divided into two major stages: initial classification of the mass (into one of the three major tumor types: cyst, semisolid, solid), and detailed analysis of the mass. Malignancy evaluation is performed based on the collected data and the criteria provided by commonly used scoring systems. The results reflect adequate performance of the automatic method developed (referring to clinical requirements). (E-mail: solange@post.tau.ac.il) © 2003 World Federation for Ultrasound in Medicine & Biology.

Key Words: **Ovarian masses, Morphological scoring, Gray scale sonography, Image processing, Malignancy evaluation.**

INTRODUCTION

Ovarian masses are common among women of all ages. Moreover, ovarian cancer is an intractable and lethal disease that is hardly detectable in the early stages. An efficient way for classifying ovarian masses and detecting malignant tumors may improve both the diagnosis and the efficiency of the treatment. Furthermore, such a method may be used in the future for real-time tumor diagnosis during surgery.

Cysts are the most common ovarian pathology. Most of them are benign, but some are malignant. The fluid within a cyst may be either transparent, appearing dark in the ultrasound (US) image, or turbid. Cysts may also contain papillations or be divided to several parts by septations. The regularity and thickness of the wall, as well as the size of the cyst, are also important for diagnosis.

Solid masses are another class of ovarian pathologies. Although some of them are benign (*e.g.*, solid teratoma, fibroma), many of them are malignant. Contrary to cysts, solid masses appear as lumps of echogenic material within the ovary. In addition to their size, important parameters are the homogeneity of the solid material and the presence of echogenic foci. There are cases in which the ovarian mass encompasses a cyst and solid tissue. Such cases are defined as semisolid masses.

The major attempts to automatically analyze ovarian US images involved only ovarian follicles (Muzzolini et al. 1993, 1994, 1998; Potocnic et al. 1997; Viher et al. 1997; Krivanek and Sonka 1998; Sarty et al. 1998). One approach (Jiang and Chen 1998) discriminated between abnormal ovarian regions and normal ones. A computerized system for quantification of ovarian masses, however, must deal with more complex ovarian morphology. Currently, no published research fully addresses this problem, and no clinical use of such an approach is known of.

Two powerful tools in the area of medical diagnosis are expert systems and artificial neural networks. Brüning et al. (1997) presented an expert system called ADNEXPERT, which is specifically designed to assist the sonographic diagnosis of adnexal tumors. Similarly, Tailor et al. (1999) and Biagiotti et al. (1999) presented neural network algorithms that assess the malignancy of adnexal tumors based on their sonographic features. However, both techniques perform differential diagnosis

Address correspondence to: Solange Akselrod, Ph.D., Medical Physics Department, Tel Aviv University, Tel Aviv 69978 Israel. E-mail: solange@post.tau.ac.il

of adnexal masses based on data manually provided by the physician. Thus, these methods automate only the final decision-making step of tumor evaluation.

A commonly used quantitative tool for malignancy detection in the ovary is scoring systems (Finkler et al. 1988; Sassone et al. 1991; DePriest et al. 1993; Lerner et al. 1994; Kurjak and Predanic 1992). The basic idea was to score several properties of the ovarian mass, according to a predetermined table, and to use the result (the sum of the individual scores) for classification. Some of the scoring systems (Finkler et al. 1988; Sassone et al. 1991; DePriest et al. 1993; Lerner et al. 1994) are based solely on morphologic features of the mass obtained from B-scans, while others (Kurjak and Predanic 1992) incorporate parameters obtained from sources such as Doppler images. Although these scoring systems reasonably succeeded in sorting the ovarian mass to either benign or malignant, they were all based on subjective evaluations made by the operator. No existing scoring system is currently based on either automatic or semiautomatic analysis of US images.

In this work, an automatic technique for quantitative analysis and malignancy detection of ovarian masses using B-scan US images is presented. The computerized analysis concentrates on morphologic classification and quantitative evaluations of the tumor, yielding a set of features that describe the morphology of the tumor. These automatically obtained data are then used by the algorithm to evaluate the malignancy of the tumor (similar to a scoring system). Apart from a single step performed by the user at the beginning of the process, the algorithm is entirely automatic.

MATERIALS AND METHODS

Image and data acquisition

This work is based on the analysis of B-scan transvaginal ultrasonic images generated by a commercial scanner. The images were partly obtained using the Acuson 128XP/10 scanner (Acuson, Mountain View, CA) with a 5- to 7-MHz transvaginal probe. The rest were generated by the Aloka SSD-680 (Aloka, Tokyo, Japan) with a 5-MHz transvaginal probe. All these images were recorded on video cassettes (VHS format), and later digitized into the computer using a DT-2853 frame grabber (Data Translation, Marlboro, MA), yielding images containing 512 pixels $\times$ 512 pixels $\times$ 256 grey levels.

The performance of initial classification was tested using a set of 163 images; the tested region-of-interest (ROI) was selected manually from each image. In 131 images taken from this series, testing was also performed after automatic determination of the ROI. The division of the above image set into tumor types is provided in Table 3 (see the Results section). Detailed tumor analysis was evaluated both for cysts and for other tumors; the segmentation algorithm for cysts was tested on 42 images (28 transparent cysts and 14 turbid cysts), and the analysis of noncystic masses was assessed using a group of 36 images (8 solid masses and 28 partly solid masses). Malignancy evaluation was checked using a set of 28 images.

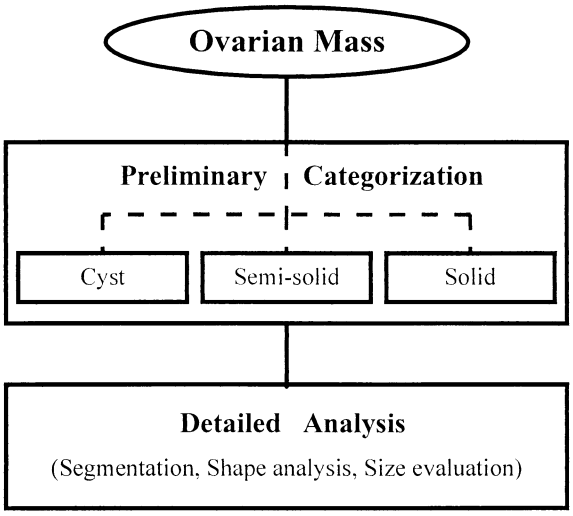

Fig. 1. The main stages of morphologic analysis.

The entire analysis approach and all algorithms involved were developed on a Silicon Graphics workstation, using C programming as well as standard software packages such as Matlab.

Overview of the algorithm

The core of the technique is a morphologic analysis of the ovarian mass. The method designed for this task is divided into two major stages: initial classification of the mass, and detailed analysis of the mass (see Fig. 1). The analyzed region (*i.e.*, the tumor) is automatically determined by a preceding step.

The first stage basically categorizes the mass into one of the three major tumor types (cyst, semisolid, solid), based on the statistical properties of the mass (as seen in the image). In this step, we define a set of statistical parameters, present them in feature space, and categorize the tumors using decision rules. Essentially, the parameters we use are the mean grey level, its standard deviation (SD), and the coefficient of variation (noise-to-signal ratio) of the grey level.

The second stage is a detailed (*i.e.*, quantitative) analysis of the mass. In this part of the procedure, different processing chains are applied to the image, depending on the former initial classification. Initially, the

already extracted information on the mass is further analyzed for refined tumor classification. This substep enables separating transparent cysts from turbid ones, and identifying some specific tumors of clinical importance. Then, a specifically designed algorithm for the detailed analysis is applied to each tumor, according to its type. Cysts are segmented (Zimmer et al. 1996) and the structures within them are classified and quantitatively evaluated (Zimmer et al. 1999). The algorithm, thus, extracts the quantitative information about the cyst (the number and diameters of papillations, the number and widths of septations, the tumor size). For solid tumors and some preidentified specific ones (*e.g.*, endometrioma), only the tumor size has to be evaluated. For semisolid ones, the size, composition (relative parts of solid and cystic materials), and the structure of the cystic parts must be evaluated. The last item is essentially addressed using the algorithm designed for the analysis of cysts.

The final step in the analysis is malignancy evaluation, which is performed based on the collected data and the criteria provided by published scoring systems.

Determination of the region-of-interest

To obtain an initial ROI, the operator draws an ellipse roughly encircling the ovary. This is the only nonautomatic step in the procedure. Then, this ellipse is automatically intersected with the previously generated template of the US sector (which is basically predetermined by the specific US scanner). This intersection provides an ROI that approximately overlaps the ovary and is fully contained within the sector. Because our aim is an ROI containing only the tumor, the boundary of the tumor is then identified by searching within the ovary.

First, four different boundary maps are generated from the original image. The values for each pixel are computed in a small square window around the pixel (in our case, 11 × 11 pixels). The four images obtained display the following parameters:

1. The "morphologic" gradient = the difference between the maximal grey level and the minimal one in the window. This variable is, in fact, the gradient (in absolute values) of the pixel when computed using mathematical morphology.
2. The local coefficient of variation (L-CV) = the SD of the grey level in the window, divided by the mean grey level there.
3. The local grey-level entropy, which is defined as follows:

$$\text{ent} = -\sum_{g=0}^{L} P_g \ln(P_g) \tag{1}$$

(where P_g = the probability of having a grey level g in a small window around the pixel, and L = the maximal possible grey level).

4. The Hurst coefficient = a parameter linearly related to the fractal dimension. The idea is to compute the average grey-level difference between all possible pixel pairs located at a specific distance from each other, repeating this process for a set of different distances (Chen et al. 1989; Wu et al. 1992). This grey-level difference is related to the associated distance by a power law rule, with the power being the Hurst coefficient.

   If we denote the grey-level difference ΔI for a distance Δx as $\Delta I_{\Delta x}$, then the above power law is written as

$$\Delta I_{\Delta x} = K \cdot \Delta I^H \tag{2}$$

   where H is the Hurst coefficient and K is a constant. The Hurst coefficient itself is defined as $H = 3 - D$, where D is the fractal dimension.

After computing these four edge maps, radial search in 256 directions is performed in each one of them within the ROI from the center of the mass, and a set of 256 candidate boundary points is collected for each parameter. The candidate boundary points were selected as the pixels with maximal value along the outer half of each scanning (*i.e.*, radial) line. For each search direction, the four points obtained (one from each set) were replaced by their median; hence, yielding a single set of boundary points. (The median of four values is the mean of the two values left when the smallest and largest ones are excluded.) Finally, by connecting these points, the curve that represents the boundary of the tumor is generated and smoothed. The ROI representing the ovarian tumor is, thus, determined.

Initial classification of the tumor

Initial classification into tumor types is performed using four different variables, evaluated in the ROI containing only the tumor. These four variables are:

1. The SD of the grey level in the entire ROI
2. The slope of the local CV (slope of L-CV). The L-CV is defined as before (*i.e.*, the grey-level SD in a window divided by the mean grey level there). This variable was computed for windows with sizes 5, 7, 9, 11, 13 and 15 pixels around the examined pixel. Then, linear regression was performed on the set of obtained CVs as a function of the various window sizes. The slope obtained is the parameter utilized.
3. The coefficient of variation (CV) in the entire ROI

Table 1. The decision rules

SD	Slope of L-CV	CV	Mean *g*	Conclusion
<5	Any value	Any value	Any value	Transparent cyst
5–10	<0.40	<0.6	Any value	Transparent cyst
	>0.40	<0.6	Any value	Turbid cyst
10–15	<0.45	<0.6	<50	
	0.45–0.50	<0.6	<70	Turbid cyst
	>0.50	<0.6	Any value	
		Else (CV <0.6)		Dense cyst/significantly solid
15–20	>0.50	<0.6	>70	Solid
		Else (CV <0.6)		Dense cyst/significantly solid
20–25	<0.50	<0.6	Any value	Dense cyst/significantly solid
	>0.50	<0.6	Any value	Significantly solid
>25	Any value	<0.6	Any value	Significantly solid
>5	Any value	>0.6	Any value	Semisolid

dense cyst = a turbid cyst with dense fluid; significantly solid = semisolid (with either separate or mixed cystic and solid parts), dermoid, solid; *g* = grey level.

4. The mean grey level in the entire ROI.

Using the above four variables and an ROI containing only the tumor, a classification scheme was obtained. The set of decision rules we used is presented in Table 1. (It should be clarified that the values provided in Table 1 were obtained empirically and the decision boundaries were deliberately chosen to be as "round" as possible.)

The ROIs used for designing the decision rules were manually determined rectangles that contained only the tumor, while the tumor type classification itself was performed on automatically obtained ROIs. To avoid bias, the average values of the global variables (*i.e.*, all variables except the slope of L-CV) were replaced by median values. The three new variables were: median (g); 'SD'(g) = median(|g − median(g)|); 'CV' = 'SD'(g)/median(g). The values obtained from these modified variables were applied to the set of decision rules constructed by the original variables.

Analyzing a cyst

The detailed analysis of an ovarian cyst starts with separating it from the rest of the image. Segmentation performs this task because it yields an image in which the ovarian cyst is represented by one grey level and its surrounding tissue is represented by a different grey level. The segmentation technique we used (Zimmer et al. 1996) is a bivariate extension of a previously used thresholding method (Li and Lee 1993) known as "minimum cross-entropy thresholding" (MCE). This extension employs a linear combination of the grey level and the local entropy (instead of using only the grey level). Because, in US images, the local entropy is correlated with the local brightness, it can be used for the segmentation of ovarian cysts.

Figure 2 provides two examples of image segmentation. The top row shows a transparent cyst while the bottom one shows a turbid cyst. In each row, the left image is the original B-scan and the right image is the segmented one.

Important features of an ovarian cyst are the absence or presence of various structures within it and their properties. Quantification of such structures (namely, papillations and septations) is an extremely important part in the detailed analysis of ovarian cysts. We developed an algorithm (Zimmer et al. 1999) that categorizes the structures within a cyst and extracts their quantitative geometrical properties (width, characteristic diameter), based on the previously obtained segmented image.

The developed algorithm (Zimmer et al. 1999) first computes the convex hull of the shape representing the cyst, and uses it to isolate the various structures. Each

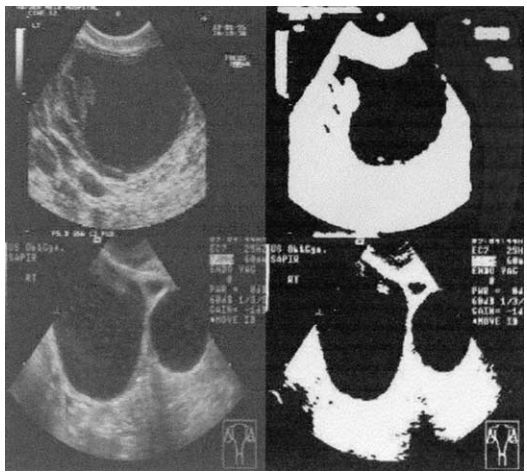

Fig. 2. Image segmentation. (top) Transparent cyst, (bottom) turbid cyst. In each row: (right) original image, (left) segmented image.

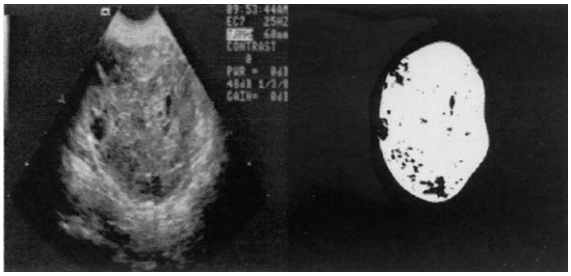

Fig. 3. Image segmentation of a partly solid tumor. (left) original image, (right) segmented tumor.

structure is then identified based on its geometrical properties using minimum error rate Bayes classification. Finally, quantitative evaluation of the characteristic width (for septations) or diameter (for papillations) of the structure is performed using mathematical morphology. For complete septations, the applied technique is simpler and the same parameter (*i.e.*, the septation width) is computed (Zimmer et al. 1999).

Analyzing tumors with a dominant solid component

The detailed analysis performed on semisolid and solid masses is relatively simple. Only the tumor size and its composition (relative parts of solid and cystic materials) are usually the parameters of interest. When required, the structure of the cystic parts can also be analyzed using the algorithm designed for cysts.

The size of the tumor can be easily estimated from the ROI containing the tumor (which was already defined at a previous stage of the algorithm). The partition between cystic and solid materials can be estimated by thresholding the image and mapping the dark and bright regions in the binary image. Thresholding was performed using the simple empirical rule that a pixel is bright (*i.e.*, "solid") when its grey value reaches 50 and the SD of the grey levels in an 11×11 window around it reaches the value 10.

Figure 3 demonstrates image segmentation of a semisolid tumor. The left image is the original B-scan and the right image is the segmented tumor.

Malignancy evaluation

The ultimate goal in analyzing an ovarian mass is to evaluate the malignancy of the tumor. For that purpose, we constructed a scoring table derived from previously published scoring systems (Sassone et al. 1991; DePriest et al. 1993; Kurjak and Predanic 1992) and adapted to the set of features measured by our algorithm. This simplified scoring system is provided in Table 2.

As shown in Table 2, the four properties used for scoring are the relative solid part in the tumor, presence and size of papillations, presence and width of septations, and the tumor size.

The first parameter, the relative solid part in the mass, is actually computed only for tumors that appear to be partly solid (according to Table 1). For transparent cysts, this parameter is assumed to be "minimal" (*i.e.*, almost no solid content at all). For turbid cysts, the definition "very low" is used. Finally, for solid masses, the relative solid part is assumed to be "high."

The wall structure, expressed by the presence and size of papillations and septations, is also implemented (as two different parameters) in our scoring system. The value of 3 mm, separating small from large papillations and thin from thick septations, is used in accordance with the convention in scoring systems. For partly solid tumors, the value 2 was automatically assigned as the sum of the scores for "papillations" and "septations." This reflects the common situation of the existence of thick septations and no papillations in such tumors, and prevents the need for the tedious task of analyzing each cystic cavity in the mass.

The size of the tumor is defined as either "small" (area smaller than 2000 mm^2) or "large" (area larger than 2000 mm^2). The bounding value approximately describes a circle of radius 25 mm. Hence, an average tumor diameter of 50 mm is taken as the threshold between small tumors and large ones. The area itself is calculated by pixel counting.

Following the published scoring systems, the final score assigned to the tumor is the sum of the scores obtained for the above-detailed properties of the tumor.

RESULTS

Initial classification

To assess the performance of initial classification, we used a set of 163 images. An ROI containing the tumor itself (*i.e.*, containing a portion of it that is a good representation of the tumor features) was manually se-

Table 2. The scoring system

	0	1	2	3	4
Solid part	Minimal	Very low	Low (<33%)	Medium (33–66%)	High (>66%)
Papillations	None	Small (<3 mm)	Large (>3 mm)		
Septations	None	Thin (<3 mm)	Thick (>3 mm)		
Tumor size	Small (<2000 mm^2)	Large (>2000 mm^2)			

Table 3. Performance of initial classification

Tumor type	Automatically obtained ROI		Manually obtained ROI	
	n of images	Success rate (%)	*n* of images	Success rate (%)
Transparent cyst	21	81.0	25 (21)	88.0 (85.7)
Turbid cyst	47	89.4	67 (47)	85.1 (87.2)
Significantly solid	45	68.9	50 (45)	92.0 (95.6)
Solid	18	72.2	21 (18)	100.0 (100.0)
Total	131	78.6	163 (131)	87.7 (91.6)

lected from each image. On this set of manually obtained ROIs ("ideal" regions), we applied the calculations and decision rules described in Table 1. In addition, 131 images taken from this series were subjected to the automatic preliminary step of determining the ROI (manual tracing of an ellipse, automatically identifying the tumor boundaries) before testing the classification algorithm on them. The results obtained for both cases are provided in Table 3. The figures in parentheses refer to the same subgroup of 131 taken from the set of 163 images.

Table 3 shows that, for cysts, the algorithm succeeds in correctly classifying the tumor in more than 80% of the cases. For the solid and partly solid masses, the success rate is about 70%. However, almost all the cases are correctly classified when an ideal ROI (*i.e.*, a rectangle containing a representative portion of the tumor) is used. Hence, the set of decision rules itself performs well for both cystic and solid-dominated tumors.

Analyzing a cyst

The next step to test is the segmentation process, applied to cysts. For that purpose, we compared segmented images (both when the entire algorithm was automatic and when the ROI was a manually obtained "ideal" rectangle containing similar portions of the cyst and its surrounding) to manually traced boundaries of the cysts (outlined by an expert). For transparent cysts, segmentation was followed by adjacent erosions with a 3×3 square structuring element (for the erosions; the cyst is considered dark and its vicinity bright) to avoid underestimation of the computed area. We used five erosions for images involving automatically obtained ROIs and only three erosion steps for images with manually obtained ROIs. The segmentation of transparent, as well as turbid, cysts is demonstrated in Fig. 2.

The two parameters used for performance evaluation were the (absolute) difference between the two compared areas of the cyst, and the relative part of the area that is mutual to the tested image and the manually traced one (*i.e.*, the ratio between the area within cyst in the tested image and the area of the manually traced cyst). Segmentation was tested on a set of 56 images (42 displaying transparent cysts and 14 showing turbid ones), and the results obtained are provided in Table 4.

Table 4 shows a slight change (mainly an increase for turbid cysts) in the area difference when moving from ideal ROIs to automatically obtained ones. The relative mutual area remains virtually the same for both cases (although its variance is significantly higher for automatically obtained ROIs). We can summarize that the average error in cyst segmentation, as expressed by both parameters, is roughly 10%.

The results in Table 4 indicate that the average effect of the previous steps (the ROI selection technique) on the segmentation error is minor. To test whether this statement is also valid for an individual image, we compared one by one the images processed with ideal ROIs with those processed using automatically obtained ROIs. For each image pair, we computed the change in the two above parameters (area difference, relative mutual area). We found that the change in area difference was about $0.5 \pm 5.0\%$ for transparent cysts and $-5.1 \pm 7.9\%$ for turbid cysts (we averaged the two values, not the absolute values). The change in relative mutual area was found to be about $-1.1 \pm 5.4\%$ for transparent cysts and $4.6 \pm 8.0\%$ for turbid cysts. These results are provided in Table 5.

The above results confirm that although, for some cases, the technique of selecting the ROI (manual, automatic) does affect the segmentation, in most cases this effect is quite small.

The final step in analyzing a cyst is the identification of structures within the cyst and extracting evalua-

Table 4. Performance of image segmentation

	Transparent cysts		Turbid cysts	
	Ideal ROI	Automatic ROI	Ideal ROI	Automatic ROI
Area difference (%)	8.1 ± 8.0	7.6 ± 5.9	7.9 ± 12.5	13.0 ± 10.7
Relative mutual area (%)	89.5 ± 7.0	90.6 ± 5.4	88.5 ± 12.0	83.9 ± 10.3

Table 5. Difference in test parameters using ideal and automatic ROI*

	Transparent cysts	Turbid cysts
Area difference (%)	0.5 ± 5.0	−5.1 ± 7.9
Relative mutual area (%)	−1.1 ± 5.4	4.6 ± 8.0

*Negative sign indicates that, on average, using manual ROI gave smaller errors.

tions of their characteristics. The algorithm for structure analysis and its performance using an "ideal" case (*i.e.*, manually traced boundaries of the cyst) were already published (Zimmer et al. 1999). Table 6 provides both the published results and those obtained for the automatic process.

It can be seen that, for septations, the structure identification procedure yields similar results for automatically processed and manually traced images while, for papilations and false structures, the success rates obtained for "automatic" images are significantly lower (by 15 to 20%) than the ones found for "ideal" images (*i.e.*, manually traced boundaries of the cyst).

Analyzing tumors with a dominant solid component

Next, images of masses containing significant portion of solid material were considered. For such tumors, we evaluated the accuracy of size measurement by using the group of images that was subjected to the automatic preliminary steps and initial classification, and previously used for testing the initial classification algorithm. Only images that yielded correct initial classification were used in the further validation procedure.

The tumor size in these images was automatically computed and compared to manual tracing. The results are provided in Table 7.

We see that, for solid tumors, the computed tumor size is evidently in good agreement with the manually obtained one, while the size of partly solid tumors is only a rough estimate.

To test to what extent the cyst-solid partition is accurately assessed, we used a subgroup of 19 images for which we had manually outlined the boundaries of the solid parts (taken from the above set of 28 images). We first computed the ratio between the solid part of the tumor and its entire size both for the manual results and for the automatic ones. Then, we compared those sets of values and found the mean error (*i.e.*, absolute difference) in evaluating this ratio. The results are presented in the right column of Table 7.

Table 6. Performance of structure analysis

	Success rate of structure identification (%)		Mean error of quantitative evaluation (mm)	
Structure type	Manual	Automatic	Manual	Automatic
Papillation	72.3	54.2	1.7	1.8
Septation	75.0	78.6	0.9*/0.9†	1.25*/0.95†
False structure	90.2	75.0	–	–

*incomplete septations: †complete septations.

Malignancy evaluation

To evaluate the performance of malignancy detection, we analyzed a set of 28 presurgical ultrasonographic images displaying various tumors for which histologic results were available. The entire automatic algorithm for initial classification and tumor analysis was fully applied to this image set. The results obtained were fed into our scoring system, and the malignancy of each tumor was estimated according to the score obtained. We decided to define a tumor as malignant if its score was more than 4 (empirically, this provided the best results). The results of applying the scoring process on the set of images are provided in Table 8.

It is easy to conclude, using Table 8, that 23 of the 28 tumors were correctly classified (a success rate of 82.1%). Furthermore, the sensitivity of automatic malignancy evaluation is exactly 80%, the specificity is 100%, the positive predictive value (PPV) is 100% and the negative predictive value (NPV) is 37.5%.

DISCUSSION

Initial classification

The initial classification of the tumor is an essential step that determines the subsequent analysis algorithm applied to the tumor. Table 3, which summarizes the performance of initial classification, reveals two interesting facts. First, the results achieved with manually obtained ROIs are significantly better than the ones obtained with the fully automatic algorithm. Secondly, when manually obtained ROIs are used, the success rates are higher for tumors containing (partly or only) solid tissue than for cysts, and the opposite case is observed when using the fully automatic algorithm (*i.e.*, cystic tumors exhibit higher success rates than other tumors).

The first observation (*i.e.*, better performance for manually obtained ROIs) is expected because using the fully automatic algorithm involves an additional error factor (the process of automatically finding the boundary of the tumor).

The second above-observed phenomenon is less obvious. For manually obtained ROIs ("ideal" regions), the good contrast makes it relatively easy to determine whether the mass is mainly cystic, partly solid or mainly

Table 7. Analysis of tumors with a significant portion of solid material

Tumor type	Difference in tumor size: *n* of cases	Difference (mm^2)	Difference (%)	Difference in solid part / entire tumor: *n* of cases	Difference (%)
Solid	8	376 ± 340	7.0 ± 7.0	–	–
Partly solid*	28	910 ± 985	18.3 ± 12.7	19	9.8 ± 7.6

*Including: semisolid, endometrioma, hemorrhagic cyst, dermoid.

solid. However, a cyst may be sometimes misclassified as partly solid due to noise, turbid material or small structures within the cyst that resemble solid material. This effect has no parallel in solid-containing tumors; hence, the slightly better results for such cases.

Applying the fully automatic algorithm to the image shows that the added preceding step of automatic ROI determination performs much better for cysts than for noncystic tumors. Again, we explain this fact by the larger contrast between the cyst and the surrounding tissue. Due to poorer contrast, the automatically obtained boundaries of solid-containing tumors are more sensitive to mistakes and are, thus, less accurate on average.

Analyzing a cyst

Tables 4 and 5, which summarize the performance of the image segmentation, indicate that the effect of previous steps (ROI selection technique) on the segmentation error is minor. The large SDs of the variables in Table 5 mean that, actually, there is no significant preference to either approach (manual or automatic ROI). In other words, we may ignore the effect of the previous steps on the algorithm.

Table 4 also shows that the errors obtained for turbid cysts are generally larger than the ones obtained for transparent cysts. This is explained by the lower contrast between the cyst and the surrounding tissue, which disturbs correct segmentation.

Finally, to assess the possible (rather than average) error of the tumor size or location, we must consider at least 2 SDs from the mean values. For a fully automatic algorithm, we find (using Table 4) that, in both parameters, the maximal error is about 20% for transparent cysts and about 35% or so for turbid cysts. These results are certainly reasonable for transparent cysts. For turbid cysts, we must use the values obtained with caution, but they are still within a clinically useful range.

Table 8. Results of malignancy evaluation using a scoring system

		Scoring results: Benign	Malignant
Histology	Benign	3	0
	Malignant	5	20

The results provided in Table 6 indicate that structure classification deteriorates mainly for papillations and sides, while remaining virtually the same for incomplete septations. This fact can be explained by the similar geometry of papillations and sides, which is quite different from the shape of incomplete septations. Hence, inaccurate shape analysis due to previous steps is likely to have a smaller effect on identifying incomplete septations. For complete septations, identification was trivial because they result essentially in two (or more) distinct cystic areas.

The accuracy of quantitative evaluations (mean diameter of papillations, width of septations) exhibits a slight difference between the results obtained using the manually outlined boundaries and those computed using the fully automatic algorithm.

Analyzing tumors with a dominant solid component

The analysis of significantly solid tumors yielded two parameters describing the mass; its size and the ratio between the solid part and the cystic component within the tumor. As shown in Table 7, the automatically computed size of solid tumors is in good agreement with the manual results, while for partly solid tumors the size is only roughly estimated. Furthermore, the absolute error in tumor size obtained for solid is small, so that most tumors will not be misclassfied in the scoring process (as "large" instead of "small" or *vice versa*). The absolute error (*i.e.*, deviation) for partly solid tumors is much larger, but most partly solid tumors were, nevertheless, correctly classified in the scoring step of the algorithm. The other estimated parameter, namely the relative part of solid tissue within the tumor, seems to be obtained with reasonable accuracy. Although the accuracy achieved is not sufficient for detailed analysis of the tumor, it is suitable for malignancy detection based on a scoring table.

Table 9. Performance of various morphological scoring systems

Authors	Sensitivity (%)	Specificity (%)	PPV (%)	NPV (%)
Current	80.0	100.0	100.0	37.5
Hermann et al. (1987)*	82	93	75	95
Granberg et al. (1990)*	82	92	74	95
Sassone et al. (1991)*	100	83	37	100
Kurjak and Predanic (1992)	92.1	94.8	79.5	97.7
Depriest et al. (1994)	89	73	46	96

*Data also provided by Kurjak and Predanic (1992).

Malignancy evaluation

As detailed above, we applied the entire automatic algorithm to a set of 28 images and compared our malignancy evaluation to the histologic results. Although 23 of the 28 tumors were correctly classified and although there are no false-positive results, we still have 5 false-negative results that clinically represent missed ovarian malignancies. In addition, for the set of test images, we chose only the ones whose type had been correctly classified (in the initial classification step). We, therefore, must weigh the success rate of initial classification in the current performance evaluation. Furthermore, we must remember that the small number of benign cases prevents an accurate estimate of false-positive rates. All the above suggest that our automatic malignancy evaluation can be used as an aid for the physician, but not as the sole criterion for further diagnosis and treatment. This agrees with the widely accepted approach to use both morphologic and Doppler parameters of the ovarian mass for scoring.

To further assess the performance of our scoring system, it is interesting to compare it to previously published ones. Table 9 provides a comparison to the major performance indices of several published morphologic scoring systems.

Table 9 shows that the sensitivity of our system is almost as high as those of the other scoring systems. We also achieve better specificity and PPV than the other techniques; the major drawback of our scoring algorithm seems to be its NPV. Yet, we must recall that we assess all the scored variables automatically from the US images (unlike the other studies), and also that our performance analysis is based on a limited number of samples.

We conclude, from the above comparison, that the performance of the automatic malignancy evaluation in this research is reasonable. Still, the relatively high level of false-positive results means, at this point, that it cannot function as an expert system (*i.e.,* used as the sole source for medical decision), but only as a decision support system.

SUMMARY

An almost automatic technique for the analysis and classification of ovarian masses is presented in this paper. The algorithm first analyzes the ovarian mass automatically using an US image, and then uses the extracted data to evaluate the malignancy of the tumor. Image analysis begins with initial classification of the mass into one of the major tumor types, followed by detailed morphologic analysis of the tumor. Apart from a small amount of information (rough ROI) provided by the user in the beginning of the process, the algorithm is entirely automatic.

Initial classification yielded a success rate of 80 to 90% for cysts and about 70% for solid-containing tumors. The size of cysts was computed with an average error of 10%, and the characteristic size of cystic structures was evaluated with an error of 1 to 2 mm on average. The size of solid-containing tumors was evaluated with an average error of 7% for solid masses and about 18% for partly solid masses. Malignancy was detected with a success rate of 82%, and our scoring table proved to be comparable to previously published morphologic scoring systems.

Overall, the algorithm performs well and automatically provides information about tumor morphology as well as an evaluation of its malignancy. We see this algorithm as the basis of a decision support system that may assist the medical expert in the diagnosis of ovarian masses. The quantitative information obtained on the tumor can also be fed into an existing (or future) expert system; thus, making its data-collecting phase automatic.

Acknowledgments—This work was supported by a grant from the Israeli Ministry of Science and by the Abramson Center for Medical Physics.

REFERENCES

Biagiotti R, Desii C, Vanzi E, Gacci G. Predicting ovarian malignancy: Application of artificial neural networks to transvaginal and color Doppler flow US. Radiology 1999;210:399–403.

Brüning J, Becker R, Entezami M, et al. Knowledge-based system ADNEXPERT to assist the sonographic diagnosis of adnexal tumors. Methods Inf Med 1997;36:201–206.

Chen CC, Daponte JS, Fox MD. Fractal feature analysis and classification in medical imaging. IEEE Trans Med Imag 1989;8:133–142.

DePriest PD, Van Nagell JR, Gallion HH, et al. Ovarian cancer screening in asymptomatic postmenopausal women. Gynecol Oncol 1993; 51:205–209.

DePriest PD, Varner E, Powell J, et al. The efficacy of a sonographic morphology index in identifying ovarian cancer: A multi-institutional investigation. Gynecol Oncol 1994;55:174–178.

Finkler NJ, Benacerraf B, Lavin PT, Wojciechowski C, Knapp RC. Comparison of serum CA 125, clinical impression, and ultrasound in the preoperative evaluation of ovarian masses. Obstet Gynecol 1988;72:659–664.

Granberg S, Norstrom A, Wikland M. Tumors in the lower pelvis as imaged by vaginal sonography. Gynecol Oncol 1990;37:224.

Hermann IJ Jr, Locher GW, Goldhirsh A. Sonographic patterns of ovarian tumors: Prediction of malignancy. Obstet Gynecol 1987; 69:777.

Jiang CF, Chen ML. Segmentation of ultrasonic ovarian images by texture features. Proceedings 20th Annual International Conference of the IEEE Engineering in Medicine and Biology Society (EMBS), Oct. 29–Nov. 1, 1998, Hong Kong, China. Proc IEEE Eng Med Biol 1998;20(2):850–853.

Krivanek A, Sonka M. Ovarian ultrasound image analysis: Follicle segmentation. IEEE Trans Med Imaging 1998;17:935–944.

Kurjak A, Predanic M. New scoring system for prediction of ovarian malignancy based on transvaginal color Doppler sonography. J Ultrasound Med 1992;11:631–638.

Lerner JP, Timor-Tritsch IE, Federman A, Abramovich G. Transvaginal ultrasonographic characterization of ovarian masses with an improved, weighted scoring system. Am J Obstet Gynecol 1994; 170:81–85.

Li CH, Lee CK. Minimum cross entropy thresholding. Pattern Recog 1993;26:617–625.

Muzzolini R, Yang YH, Pierson R. Multiresolution texture segmentation with application to diagnostic ultrasound images. IEEE Trans Med Imaging 1993;12:108–123.

Muzzolini R, Yang YH, Pierson R. Texture characterization using robust statistics. Pattern Recog 1994;27:119–134.

Muzzolini R, Yang YH, Pierson R. Classifier design with incomplete knowledge. Pattern Recog 1998;31:345–369.

Potocnic B, Zazula D, Korze D. Automated computer-assisted detection of follicles in ultrasound images of ovary. Proceedings of the Tenth IEEE Symposium on Computer-Based Medical Systems, 11–13 June 1997, Maribor, Slovenia. Los Alamitos: IEEE Computer Society Press, 1997:16–21.

Sarty GE, Liang W, Sonka M, Pierson RA. Semiautomated segmentation of ovarian follicular ultrasound images using a knowledge-based algorithm. Ultrasound Med Biol 1998;24:27–42.

Sassone AM, Timor-Tritsch I, Artier A, Westhoff C, Warren WB. Transvaginal sonographic characterization of ovarian disease: Evaluation of a new scoring system to predict ovarian malignancy. Obstet Gynecol 1991;78:70–76.

Tailor A, Jurkovic D, Bourne TH, Collins WP, Campbell S. Sonographic prediction of malignancy in adnexal masses using an artificial neural network. Br J Obstet Gynaecol 1999;106:21–30.

Viher B, Dobnikar A, Zazula D. Follicle recognition in ultrasound images using the cellular automata. Proceedings of the Tenth IEEE Symposium on Computer-Based Medical Systems, 11–13 June 1997, Maribor, Slovenia. Los Alamitos: IEEE Computer Society Press, 1997:34–39.

Wu CC, Chen YC, Hsieh KS. Texture features for classification of ultrasonic liver images. IEEE Trans Med Imag 1992;11:141–152.

Zimmer Y, Tepper R, Akselrod S. A two-dimensional extension of minimum cross-entropy thresholding for the segmentation of ultrasound images. Ultrasound Med Biol 1996;22:1183–1190.

Zimmer Y, Tepper R, Akselrod S. Computerized quantification of structures within ovarian cysts using ultrasound images. Ultrasound Med Biol 1999;25:189–200.